

# Relations Between Timing Features and Colors in the X-Ray Binary 4U 0614+09

Steve van Straaten<sup>1</sup>, Eric C. Ford<sup>1</sup>, Michiel van der Klis<sup>1</sup>, Mariano Méndez<sup>1,2</sup>, Philip Kaaret<sup>3</sup>

## ABSTRACT

We study the correlations between timing and X-ray spectral properties in the low mass X-ray binary 4U 0614+09 using a large (265-ks) data set obtained with the Rossi X-ray Timing Explorer. We find strong quasi-periodic oscillations (QPOs) of the X-ray flux, like the kilohertz QPOs in many other X-ray binaries with accreting neutron stars, with frequencies ranging from 1329 Hz down to 418 Hz and, perhaps, as low as 153 Hz. We report the highest frequency QPO yet from any low mass X-ray binary at  $1329 \pm 4$  Hz, which has implications for neutron star structure. This QPO has a  $3.5 \sigma$  single-trial significance, for an estimated 40 trials the significance is  $2.4 \sigma$ . Besides the kilohertz QPOs, the Fourier power spectra show four additional components: high frequency noise (HFN), described by a broken power-law with a break frequency between 0.7 and 45 Hz, very low frequency noise (VLFN), which is fitted as a power-law below 1 Hz, and two broad Lorentzians with centroid frequencies varying from 6 to 38 Hz and 97 to 158 Hz, respectively. We find strong correlations between the frequencies of the kilohertz QPOs, the frequency of the 6–38 Hz broad Lorentzian, the break frequency of the HFN, the strength of both the HFN and the VLFN and the position of the source in the hard X-ray color vs. intensity diagram. The

---

<sup>1</sup>Astronomical Institute, “Anton Pannekoek”, University of Amsterdam, Kruislaan 403, 1098 SJ Amsterdam, The Netherlands.

<sup>2</sup>Facultad de Ciencias Astronómicas y Geofísicas, Universidad Nacional de La Plata, Paseo del Bosque S/N, 1900 La Plata, Argentina.

<sup>3</sup>Harvard-Smithsonian Center for Astrophysics, 60 Garden Street, Cambridge, MA 02138, USA.

frequency of the 97–158 Hz Lorentzian does not correlate with these parameters. We also find that the relation between power density and break frequency of the HFN is similar to that established for black hole candidates in the low state. We suggest that the changing mass accretion rate is responsible for the correlated changes in all these parameters.

*Subject headings:* accretion, accretion disks — black holes — stars: individual (4U 0614+09) — stars: neutron — X-rays: stars

## 1. Introduction

Accretion in neutron star low mass X-ray binaries can be studied through the spectral and timing properties of the associated X-ray emission. Some of these systems exhibit quasi-periodic oscillations with frequencies ranging from a few hundred Hz to more than 1000 Hz (kilohertz QPOs). These oscillations have been observed with Rossi X-ray Timing Explorer (RXTE; for reviews and references see van der Klis 1998, 1999; Swank 1998 and <http://www.astro.uva.nl/~ecford/qpos.html>). The high frequency of these signals nearly certainly reflects the short dynamical time scale in the region near the compact object where they originate. The timing properties at low frequencies ( $\nu < 100$  Hz) as well as the spectral properties are the basis of a classification of the systems as *Z* or *Atoll* sources (Hasinger & van der Klis 1989). The low frequency part of the Fourier power spectra of the atoll sources is dominated by two features (first identified with the EXOSAT satellite): a power-law red noise component in the lowest range of the spectrum ( $\nu < 1$  Hz) called very low frequency noise (VLFN), and a high frequency noise (HFN) component which is flat at low frequency and breaks to follow a power-law with an index of about 1 at higher frequency. In some cases, a low frequency Lorentzian is also seen (e.g. Wijnands & van der Klis 1999a). The HFN is very similar in shape to the low state noise of the black hole candidates (BHCs; van der Klis 1994a; Yoshida et al. 1993). Also the correlation between the break frequency of the HFN and the centroid frequency of the low frequency Lorentzian is the same for black hole candidates and neutron stars (Wijnands & van der Klis 1999a).

These timing properties are connected with

the properties of the X-ray energy spectrum. This is seen very clearly in the *Z* sources both for the lower frequency features (e.g., van der Klis et al. 1985; Hasinger & van der Klis 1989; Wijnands et al. 1997a; Kuulkers et al. 1997; Kuulkers et al. 1996) and for the kilohertz QPOs (van der Klis et al. 1996; Wijnands et al. 1997b; Jonker et al. 1998). Similar correlations exist for atoll sources as well, both for the lower frequency features (e.g., Hasinger & van der Klis 1989; Prins & van der Klis 1997; Méndez et al. 1997) and for the kilohertz QPOs (e.g., Ford et al. 1997b; Kaaret et al. 1998; Méndez et al. 1999). Also connections have been made between the frequency of the kilohertz QPOs and the frequencies of the lower frequency features (van der Klis et al. 1996; Ford & van der Klis 1998; Wijnands & van der Klis 1998). The most obvious reason for all these correlations is that the changing mass accretion rate causes changes in the timing and spectral properties (Hasinger & van der Klis 1989).

4U 0614+09 has been studied previously with EXOSAT (Singh & Apparao 1994; Barret & Grindlay 1995). The EXOSAT data showed an anti-correlation of high and low energy emission (Barret & Grindlay 1995), and observation with the Burst and Transient Source Experiment (BATSE) and the RXTE all-sky monitor showed that this anti-correlation extends to about 100 keV (Ford et al. 1996). X-ray bursts from 4U 0614+09 were identified by OSO-8 (Swank et al. 1978) and WATCH (Brandt et al. 1992; Brandt 1994). The only previously published study investigating the broadband ( $\sim 0.03$ –1200 Hz) X-ray power spectra is the Méndez et al. (1997) study of 14 ks of RXTE data, concluding that this source can be classified as an atoll source. Strong kilohertz QPOs were

discovered in this source with RXTE (Ford et al. 1997a). The frequency of these QPOs correlated with count rate over short time scales, but on long time scales this correlation broke down (Ford et al. 1997a; Méndez et al. 1997). A more robust correlation was shown to exist between the frequency and either the flux of a spectral component, the X-ray spectral shape, or a hardness ratio (Ford et al. 1997b; Kaaret et al. 1998; Méndez et al. 1997). The physical implication is that both these latter parameters and the frequency of the kilohertz QPOs are determined by a changing mass accretion rate. The 265 ks of RXTE data we use here includes 75 ks previously used by Ford et al. (1997a;1997b) and Kaaret et al. (1998) and 14 ks by Méndez et al. (1997).

In this paper we show a connection between the changes in spectral shape and both the kilohertz QPOs and the lower frequency features in a large RXTE data set for 4U 0614+09. In §2 we describe our analysis of the spectral and timing data. In §3 we present our results and in §4 we compare our results to other atoll sources and discuss the connections to physical models.

## 2. Observations and Data Analysis

In this analysis we use data from RXTE’s proportional counter array (PCA; for more instrument information see Zhang et al. 1993). The total observing time is about 265 ks, approximately 75% of the total RXTE observing time on 4U 0614+09 to date. Data sets are split into near continuous time intervals of approximately 2500 s which we shall call observations. These observations are listed in Table 1. We use the 16-s time-resolution Standard 2 mode to calculate the colors (as defined below) and the 122- $\mu$ s time-resolution Event and 0.95- $\mu$ s time-resolution Good Xenon modes

for Fourier analysis. No X-ray bursts were observed in this data set.

We calculate a hard color, defined as the count rate in the energy band 9.7–16.0 keV divided by the rate in the energy band 6.0–9.7 keV, and a soft color, defined as the count rate in the energy band 3.5–6.0 keV divided by the rate in the energy band 2.0–3.5 keV. We also calculate the intensity, the count rate over five detectors in the energy band 2.0–16.0 keV. To obtain the count rates in these exact energy ranges we interpolate linearly between count rates in the PCA channels. We calculate the colors and intensity first for each time interval of 16 s. We subtract the background contribution in each band using the standard background model for the PCA version 2.1b. We then calculate the average and standard deviation for each observation among the 16 s points. In the left panel of Figure 1 we show a diagram of hard color vs. intensity, in the right panel a diagram of hard color vs. soft color. Each point in the plot corresponds to the average of the 16 s points in one observation. The error bars indicate the standard deviation from the 16 s intervals. In the few observations where only three or four of the five PCUs were on, we normalize the count rates to five detectors.

Most of the data fall on one curve. However, there is a set of points in the 0.4 – 0.5 hardness range that appears to be shifted to higher count rate. These are the points from the 1997 observations. There is no obvious reason for the shift. The general trend in the soft color vs. hard color diagram is the same as in the diagram of hard color vs. intensity including the offset of the 1997 points. We use the diagram of hard color vs. intensity in this source instead of the color-color diagram, as was done with 4U 1608–52 (Méndez

et al. 1999) and 4U 1728–34 (Méndez & van der Klis 1999), because there is less scatter in count rate than in soft color.

Most of our observations occurred in gain *epoch 3* (between 1996 April 15 and 1999 March 22). Four of our observations (a total of 9.4 ks of data) took place in gain *epoch 1* (before 1996 March 21), two (5 ks) in gain *epoch 2* (1996 March 21 – 1996 April 15) and two (6.9 ks) took place in gain *epoch 4* (1999 March 22 to present). In order to correct the colors for these data for the changes in instrumental response, we calculate colors of the Crab nebula, which can be supposed to be constant in its colors, using the same energy bands in the various gain epochs and calculate a correction factor which we apply to the data in epochs 1, 2, and 4 to make the Crab colors match those of epoch 3 (c.f. Kuulkers et al. 1994). The correction factor for hard colors for epochs 1, 2 and 4 is about 0.2 %, 1.0 % and 0.2 % respectively. The correction factor for soft colors for epochs 1, 2 and 4 is about 3.5 %, 1.0 % and 20 % respectively. Finally, the correction factor for intensities for epochs 1, 2 and 4 is about 1.0 %, 6.0 % and 2.0 % respectively. We have tested the validity of these corrections for epochs 1 and 2 by using spectral fits of 4U 0614+09 observations and the response matrices to calculate cross-epoch corrections. The correction factors obtained in this way are within 1.5 % larger in hard color, within 7 % larger in soft color and within 10 % smaller in intensity as the Crab-based corrections.

We parametrize the position of each observation in the hard color vs. intensity diagram by a variable,  $S_a$ , which measures the distance along the curve traced out by the data (see Figure 1). This is inspired by the work on Z sources where the distance along the Z

track in the color–color diagram is parameterized by  $S_z$  (Hasinger et al. 1990; Hertz et al. 1992) and by recent results on the atoll sources 4U 1608–52 (Méndez et al. 1999) and 4U 1728–34 (Méndez & van der Klis 1999). We note that these previous studies use color–color diagrams as opposed to the color–intensity diagram we use here.

In calculating  $S_a$ , we choose a few points in the hardness–intensity diagram and fit a quintic spline through these points and define  $S_a = 1$  as the point (174,0.629) and  $S_a = 3$  as the point (1255,0.295) as indicated in the figure. We rescaled the axes so that both axes range over the same values. We then find the  $S_a$  value of each observation by determining the closest point on the curve. The error in  $S_a$  is obtained by quadratically adding the errors in  $S_a$  that resulted from mapping the one sigma errors in hard color and intensity on to  $S_a$ .

We calculated power spectra from the high time resolution data. For each observation we make two spectra. One in which we use all the energy channels of the PCA, for the fit at low frequency ( $\nu \leq 400$  Hz), and one in which we apply channel cuts to select high energies for the fit of the kilohertz QPOs. The QPOs are generally stronger at higher energies. For the kilohertz QPO fits we use a nominal energy range of 4.6–97.3 keV (unbinned PCA channels 13–249 for gain epoch 3), for the other epochs we use the channel range closest to these energies. For gain epoch 1 we use channels 17–249 (4.2–68.0 keV), for gain epoch 2 channels 13–249 (3.5–75.6 keV) and for gain epoch 4 we use channels 11–219 (4.6–97.5 keV). In all cases, we divide the data into segments of 64 or 256 s and then bin the data in time before Fourier transforming such that the Nyquist frequency is always 4096 Hz.

We then average the individual power spectra over each observation. Four representative power spectra are shown in Figure 2. We fit each spectrum with a function that was found to describe all the power spectra well. The four main components are as follows. (I) The Poisson level. For the Poisson level we fit a value constant in frequency. This is valid since dead-time effects are very small in this weak source. This value is approximately 2 as expected from Poisson noise with the normalization of Leahy et al. (1983). We fit the Poisson level from 2000 to 4000 Hz, and then fix it and fit the low frequency power spectra up to 400 Hz. When we fit the kilohertz QPOs we let the Poisson level float. (II) A broken power-law whose power,  $P$ , is defined as:

$$P(\nu) = \begin{cases} A\nu^{-\alpha_0} & (\nu < \nu_{\text{break}}) \\ A\nu_{\text{break}}^{\alpha_1-\alpha_0}\nu^{-\alpha_1} & (\nu > \nu_{\text{break}}) \end{cases}$$

where  $A$ ,  $\nu_{\text{break}}$ ,  $\alpha_0$  and  $\alpha_1$  are the normalization factor, break frequency and the index below and above the break. Following previous work we will refer to this component as high frequency noise (HFN; Hasinger & van der Klis 1989). (III) A power-law below 1 Hz called very low frequency noise (VLFN; Hasinger & van der Klis 1989). (IV) The kilohertz QPOs, described by Lorentzians with best-fit centroid frequencies from 153 to 1329 Hz. In one power spectrum the centroid frequencies of the QPOs fall in the same frequency range as the low frequency noise ( $\nu < 400$  Hz), in this case we include the shape of the low frequency noise in our fit of the kilohertz QPOs.

In some cases we add two additional components to the fit function : a Lorentzian with a best-fit centroid frequency between 6 and 38 Hz (FWHM 2–19 Hz), and another Lorentzian with a best-fit frequency between

97 and 158 Hz (FWHM 22–144 Hz). Other atoll sources show similar components in their power spectra, as seen with GINGA in 4U 1608–52 (Yoshida et al. 1993) and with RXTE in 4U 1705–44 (Ford, van der Klis & Kaaret 1998), 4U 1728–34 (Ford & van der Klis 1998), 4U 1820–30 (Zhang et al. 1998a), 4U 1608–52 (Méndez et al. 1999; Ford et al. 1999) and in other binaries as well (Wijnands & van der Klis 1999a; Psaltis et al. 1999). The  $\chi^2/\text{dof}$  of our fits are typically 1.0 to 1.4 with 127 to 164 degrees of freedom.

### 3. Results

The broken power-law component of the power spectra is similar to that in previous measurements in other atoll sources and black hole candidates. The rms fractional amplitude (0.1–400 Hz) ranges from 3 to 30 %. The average value of  $\alpha_0$  is close to zero ( $-0.02$ ), and the average value of  $\alpha_1$  is close to unity (0.92). There is no evidence for a second break in this component as is seen in some descriptions of the power spectra of the BHCs and the atoll source 4U 1608–52 (Yoshida et al. 1993). Above  $S_a$  values of 2, the broken power-law has a peaked shape (Hasinger & van der Klis 1989):  $\alpha_0$  is between  $-0.2$  and  $-1.6$  and  $\alpha_1$  is between 1 and 2. These power spectra could also be fitted with a broken power-law with  $\alpha_0 \sim 0$  and  $\alpha_1 \sim 1$  if we add an extra Lorentzian with a centroid frequency near  $\nu_{\text{break}}$ . The fits reported here, however, do not include this Lorentzian as it is less than  $3\sigma$  significant in most cases.

Historically other functions have been used to describe this HFN component: a cut-off power-law described by  $P \propto \nu^{-\alpha} \exp^{-\nu/\nu_c}$  (Hasinger & van der Klis 1989), or Lorentzians with a central frequency of zero Hz (Grove et al. 1994; Olive et al. 1998). We have

tried such functions, but the  $F$ -test statistics show no preference for one of the functions. We employ the broken power-law because it uses fewer free parameters (with the other functions we often need to add an extra Lorentzian with a frequency near  $\nu_{\text{break}}$ ). Fits of the correlations (see below) also have better  $\chi^2/\text{dof}$  with the broken power-law function.

The VLFN is present in some of the intervals of March, November and December 1998 (see Table 2 and Fig. 2) with rms fractional amplitude (0.01–1 Hz) between 0.5 and 3.2 %, when  $S_a \geq 2.49$  (see Table 2 and Fig. 3). This state (extremely soft with VLFN) is often referred to as the *banana* state (Hasinger & van der Klis 1989). In all but one of the observations where the VLFN was present, it is accompanied by a significant HFN component with rms fractional amplitude between 3.1 and 13.6 % (see Table 2).

The kilohertz QPO parameters (fitted in the energy range 4.6–97.3 keV) are listed in Table 1. The kilohertz QPOs have similar properties to those in other low mass X-ray binaries. The lower frequency QPO ranges from 824 Hz down to 418 Hz and, perhaps, as low as 153 Hz. The upper frequency QPO ranges from 1329 down to 449 Hz. Note that these are fits of the power spectra above 4.6 keV. We include the kilohertz QPOs when the significance based on the error in the integrated power is above  $3.0 \sigma$ . Of the kilohertz QPOs reported here, 69 % have a significance of 3.5 to  $8.9 \sigma$  and 31 % have a significance of  $3.0$  to  $3.5 \sigma$ . The QPO with the highest observed centroid frequency,  $1329 \pm 4$  Hz is  $3.5 \sigma$  significant. This significance is for a single trial (van der Klis 1989). We estimate that the number of trials is about 40 based on the width of the detection interval ( $\sim 1000$  Hz) and the width of the QPO ( $\sim$

25 Hz) at 1329 Hz. Including these trials reduces the significance to  $2.4 \sigma$ . We note that the QPO frequency of 1329 Hz deviates from the linear trend seen for the other kilohertz QPOs (Fig. 4). The break frequency in the same observation also deviates from the linear trend seen for the break frequencies at  $S_a$  below 2.3 (Fig. 3). The frequency difference between the two kilohertz QPOs is constant over a wide range in frequency in 4U 0614+09 and has a weighted average value of  $311.8 \pm 1.8$  Hz (Fig. 4). At least one QPO is present over basically the entire range of  $S_a$  (1.25 to 2.89) and in 74 of the 94 power spectra. At  $S_a \geq 2.49$  a QPO is present in 4 of 9 observations with rms fractional amplitudes ranging from 5.1 to 11.1 %. There is generally only one QPO above  $S_a$  of about 2.3 and below  $S_a$  of about 1.7. There is one exception at  $S_a = 1.25$ , where there is a QPO present at  $153 \pm 6$  Hz. However this QPO can be identified either as the lower kilohertz QPO or one of the 97–158 Hz Lorentzians (the circle point in Fig. 4 and 5) on the basis of the correlations of centroid frequency, rms fractional amplitude or FWHM with  $S_a$ . In most cases where single QPOs are observed, they can be identified as the upper (or, in one case lower) one on the basis of the correlations of centroid frequency with  $S_a$  and/or hard color. The four highest frequency features are single QPOs but are likely the higher frequency of the two QPOs based on the  $S_a$  correlation. There is, however, some ambiguity in this identification.

In 31 of the total of 94 observations we have found it necessary to include a low frequency Lorentzian at 6 to 38 Hz. We include it in the fit when the significance based on the error in its integrated power is above  $3.0 \sigma$ . This Lorentzian is seen only at low  $S_a$

and increases in frequency with  $S_a$  (Fig. 5). The rms fractional amplitude (2.4–15.9 %) decreases as the centroid frequency increases (Fig. 5). In some cases the Lorentzian is broad, in the 1996 August 8 interval for instance it has  $Q(=\nu/\text{FWHM})$  of  $1.3 \pm 0.5$ .

The final component of our fit, a Lorentzian near 100 Hz, is clearly present at a high  $S_a$  value (Fig. 5). We include it in the fit when the significance based on the error in its integrated power is above  $3.0 \sigma$  (15 observations). The best-fit centroid frequencies are between 97 and 158 Hz and the rms fractional amplitudes between 3.9 and 13.8 %. Adding it to the fit makes  $\alpha_1$  and  $\nu_{\text{break}}$  of the HFN significantly larger.

Most of the features in the Fourier spectra discussed above are correlated smoothly with the changing energy spectrum. This is summarized in Figures 3, 5 and 4 where we plot several quantities vs.  $S_a$ , which measures the changing colors. The same quantities do not correlate smoothly with count rate (in the energy band 2.0–16.0 keV). The only exception to these correlations is the frequency of the 97–158 Hz Lorentzian, which does not correlate with  $S_a$  (Fig. 5). The 97–158 Hz Lorentzians do not fit on an extrapolation of the  $S_a$  vs. frequency correlation of the 6–38 Hz Lorentzians or its harmonics, suggesting that the 97–158 Hz Lorentzian has a different physical origin.

Since many of the parameters of the power spectra fits are correlated with  $S_a$ , many of these values are correlated with each other. Two such correlations are shown in Figure 6. Both the centroid frequency of the 6–38 Hz Lorentzian,  $\nu_{\text{LFLor}}$ , and the break frequency of the HFN are correlated with the centroid frequency of the higher frequency kilohertz QPO,  $\nu_{\text{kHz}}$ . Fitting a relation  $\nu_{\text{LFLor}}$

$= A\nu_{\text{kHz}}^\alpha$ , we obtain  $\alpha = 2.46 \pm 0.07$  and  $A = 3.0(\pm 1.4) \times 10^{-6}$  (line in Fig. 6). The fit has a large  $\chi^2/\text{dof}$  of 11.6. The quoted errors use  $\Delta\chi^2 = 1.0$ .

When we plot centroid frequency of the low frequency Lorentzian vs. the break frequency, the points fall in the same region as the plot that Wijnands & van der Klis (1999a) established for the BHCs, atoll sources and the millisecond pulsar SAX J1808.4-3569. If we estimate the frequency of the lower kilohertz QPO by subtracting the average frequency difference from the upper kilohertz QPO we can plot this vs. the centroid frequency of this Lorentzian. We fit this correlation and find that to within the errors it is consistent with the correlation that Psaltis, Belloni & van der Klis (1999) found for neutron stars and black holes.

In order to compare the HFN component with that seen in BHCs (Méndez & van der Klis 1997), we also calculated the power density at the break of the broken power-law. The values from 4U 0614+09 and from the BHCs are plotted in Figure 7.

## 4. Discussion

### 4.1. Timing–Spectra Correlations and States

The previous section demonstrates connections between properties of the energy spectrum and features in the power spectra of the low mass X-ray binary 4U 0614+09. There is a strong correlation between the position in the X-ray hard color vs. intensity diagram, the frequencies of the kilohertz QPOs, the frequency of a 6–38 Hz Lorentzian, the break frequency of the HFN and the strength of both the HFN and the VLFN.

Historically the atoll sources (4U 0614+09

among them) are known to show two source states, the so-called ‘banana’ and ‘island’ states named after their shapes in the color-color diagram (Hasinger & van der Klis 1989). In the banana state there is a strong VLFN component present in the power spectra at low frequencies and the energy spectrum is soft. In the island state the power spectrum is dominated by the HFN and the energy spectrum is harder. In the present data we observe a smooth transition between the two states, indicating that these are part of a continuous sequence (Hasinger & van der Klis 1989). Similar transitions are seen in RXTE data of other atoll sources (4U 1636–53, Prins & van der Klis 1997; 4U 1705–44, Ford, van der Klis & Kaaret 1998; 4U 1820–30, Zhang et al. 1998a; 4U 1735–44, Ford et al. 1998; 4U 1608–52, Méndez et al. 1999; 4U 1728–34, Méndez & van der Klis 1999; Aql X–1, Reig et al. 1999; Méndez 1999). In 4U 0614+09 the kilohertz QPOs are present in the whole range of the X-ray color-color diagram in contrast to data sets on similar sources that indicate that the QPOs are absent at the highest  $S_a$  and possibly the lowest as well (4U 1608–52, Méndez et al. 1999; 4U 1705–44, Ford, van der Klis & Kaaret 1998; 4U 1636–53, Zhang et al. 1996, Wijnands et al. 1997c; 4U 1735–44, Wijnands et al. 1998, Ford et al. 1998; 4U 1820–30, Smale, Zhang & White 1997; KS 1731–260, Wijnands & van der Klis 1997d). At the highest  $S_a$  ( $\geq 2.49$ ) QPOs are present in 4U 0614+09 with rms fractions of 4 to 8 % in the total energy range (5 to 11 % for an energy range of 4.6–97.3 keV). These detections are similar to previously reported upper limits for the rms fraction over the full energy range in the banana state:  $< 2-3\%$  (4U 1735–44, Wijnands et al. 1998b),  $< 2-6\%$  (4U 1705–44; Ford, van der Klis & Kaaret 1998) and  $< 1-5\%$

(4U 1608–52, Méndez et al. 1999). In 4U 0614+09 we are probably not seeing the upper banana state, where there is no HFN and the VLFN becomes very strong.

The correlation between the kilohertz QPO frequencies and  $S_a$  in this source is similar to that in the Z sources with  $S_z$  (van der Klis et al. 1996; Wijnands et al. 1997b; Jonker et al. 1998). The strength and frequency of the signals at lower frequency also show similar correlations.  $S_a$  is a much better indicator for the QPO frequencies than count rate, where a correlation with the QPO frequencies on long time scales is lacking (4U 0614+09, Ford et al. 1997a; Aql X–1, Zhang et al. 1998b; 4U 1820–30, Zhang et al. 1998a, Kaaret et al. 1999; 4U 1608–52, Méndez et al. 1999; and other sources, see Méndez 1999). Models explaining the kilohertz QPOs predict, for different reasons, that the centroid frequencies increase with mass accretion rate (Miller, Lamb & Psaltis 1998; Titarchuk, Lapidus & Muslinov 1998; Stella & Vietri 1998).

The present data indicate a link between  $S_a$  and mass accretion rate. The correlation between break frequency of the HFN and  $S_a$  further strengthens this link. The suggestion that the break frequency tracks the mass accretion rate was previously noted for atoll sources (van der Klis 1994a; Prins et al. 1997). The only possible exceptions to a correlation between break frequency and inferred mass accretion rate so far are SAX J1808.4–3658 (Wijnands & van der Klis 1998) and SLX 1735–269 (Wijnands & van der Klis 1999b) where at higher count rates the break frequency is smaller. The exception to the correlation in these sources may be related to the fact that they were observed at especially low inferred mass accretion rates. The two spectra of SLX 1735–269 have exception-

ally low break frequencies of 2.3 and 0.11 Hz (Wijnands & van der Klis 1999b). We note however, that accretion rates are inferred only from the fluxes and the relative change in flux is small, about 20 % in SLX 1735–269 and about 40 % in SAX J1808.4–3658. The anti-correlation in these sources may be due to this small dynamic range.

The changes in energy spectra, reflected in a changing  $S_a$ , are likely driven by changes in the mass accretion rate, as previously suggested for 4U 0614+09 by the correlation between the frequency of the kilohertz QPOs with the blackbody flux (Ford et al. 1997b) or with the index of the power-law (Kaaret et al. 1998). Larger values of  $S_a$  correspond to softer spectra, higher fluxes, and larger inferred mass accretion rates. From color-color diagrams, at low inferred mass accretion rate there is an anti-correlation of flux and hardness, which is manifest also in spectral studies of atoll sources: e.g., 4U 1636–53 (Breedon et al. 1986), 4U 1735–44 (Smale et al. 1986), 4U 1705–44 (Langmeier et al. 1987), 4U 1608–52 (Mitsuda et al. 1989), 4U 0614+09 (Barret & Grindlay 1995; Ford et al. 1996), and others (van der Klis & van Paradijs 1994). One long-standing explanation of this anti-correlation is in terms of thermal Comptonization models (e.g. Sunyaev & Titarchuk 1980). In the thermal model the increasing soft X-ray flux cools the Comptonizing electron plasma, leading to a decrease in its temperature and thus a decrease in hard X-ray flux.

#### 4.2. Comparison with Other Sources

The VLFN component might correspond to motion of the source along the track in the color-color diagram during an observation, as suggested for Z sources (van der Klis

1991). Observations of Cyg X–2 however indicate that the motion in the Z track is at most partly responsible for the VLFN (Wijnands et al. 1997a). Bildsten (1995) suggested that the VLFN is caused by unstable burning of nuclear fuel in a regime of time dependent helium burning. The dependence of the strength of the VLFN on the mass accretion could then be explained by a slower mode of combustion that sets in at higher mass accretion rate. This slower mode of combustion leads to stronger long time scale variations.

The 6–38 Hz Lorentzians are similar to the horizontal branch oscillations (HBOs) in the Z sources in their rms fractions and correlations with  $S_a$  and  $\nu_{\text{kHz}}$ . The HBOs sometimes show a saturation of the HBO frequency with respect to  $S_z$  at a frequency of about 60 Hz (GX 17+2, Wijnands et al. 1997b; Cyg X-2, Wijnands et al. 1998a). In 4U 0614+09 the Lorentzian frequency only goes up to 38 Hz and we do not observe a saturation of the Lorentzian frequency with respect to  $S_a$  (Fig. 5), but we do observe a saturation of the break frequency of the HFN with respect to  $S_a$  (Fig. 3).

The 97–158 Hz Lorentzians could be related to the 65–317 Hz oscillations seen in some of the black hole candidates (GRO J1655-40, Remillard et al. 1999a; XTE J1550-564, Remillard et al. 1999b; GRS 1915+105, Morgan et al. 1997). These oscillations fall in the same frequency range as the 97–158 Hz Lorentzians we observe but have weaker rms fractional amplitudes ( $\sim 1\%$ ). In GRS 1915+105 (65–68 Hz; Morgan et al. 1997) and GRO J1655-40 (281–317 Hz; Remillard et al. 1999a) the oscillations were about constant in frequency. In XTE J1550-564 however, the frequency varied considerably from 184 to 284 Hz (Homan et al. 1999; Remillard

et al. 1999a).

For what concerns the other features in the power spectra, the high frequency noise component in atoll sources is very similar to the low-state noise in black hole candidates (van der Klis 1994a,b). The BHCs show a correlation of power density at the break with break frequency (Belloni & Hasinger 1989). The relation between power density at the break and break frequency is similar in 4U 0614+09 and the BHCs in the low state (Fig. 7). However in the region where the break frequencies of 4U 0614+09 and the BHCs become comparable (the intermediate and very high state of the BHCs) 4U 0614+09 does show a larger power density. The HFN may result from a superposition of shots with the break corresponding to the shots with the longest durations, as proposed for the BHCs (e.g. Belloni & Hasinger 1990). The time scale of the shots could be set by the lifetime of clumps (van der Klis 1994b) and could decrease with mass accretion rate (Ford & van der Klis 1998).

### 4.3. Correlations of Timing Features

Stella & Vietri (1998) have proposed that the 6–38 Hz Lorentzian is caused by relativistic frame dragging in the inner accretion disk (Lense-Thirring precession). The frequency of the Lorentzian depends on the frequency of the upper kilohertz QPO, assumed to be fixed by the Keplerian frequency at the inner edge of the disk. Stella & Vietri (1998) predict a scaling index of 2, but see corrections by Morsink & Stella (1998). Our value of  $2.46 \pm 0.07$  is significantly different from 2. Also, as in 4U 1728–34 (Ford & van der Klis 1998), the required ratio of the moment of inertia over the neutron star mass is unphysically large if the nodal precession frequency is the QPO frequency. However this

is not a problem if the QPO frequency is twice the nodal precession frequency (Stella & Vietri 1998).

Titarchuk & Osherovich (1999) associate the 6–38 Hz Lorentzian with radial oscillations in a boundary layer where the disk adjusts to the rotating neutron star and the break frequency of the HFN with the diffusion time scale in this region. The correlations in 4U 0614+09 of the *lower* kilohertz QPO vs. 6–38 Hz Lorentzian and HFN break frequency do not fall on the predicted curves. In fact the correlations with respect to the *higher* frequency kilohertz QPO are closer to those predicted. In addition there is a high frequency turnover of the break frequency which is not predicted (Fig. 6).

### 4.4. The Highest Frequency QPOs

We report here the highest frequency QPO of any low mass X-ray binary to date at  $1329 \pm 4$  Hz. Such a high frequency oscillation puts new constraints on the structure of neutron stars (Miller, Lamb & Cook 1998). The mass and radius are bounded by:

$$M \leq 2.2(\nu_K/1000 \text{ Hz})^{-1}(1 + 0.75j) M_\odot$$

and

$$R \leq 19.5(\nu_K/1000 \text{ Hz})^{-1}(1 + 0.2j) \text{ km}$$

where  $j$  is the dimensionless angular momentum of the star,  $j \equiv 2\pi c I \nu_{spin} / GM^2$  (e.g. Miller, Lamb & Psaltis 1998). This expansion in  $j$  is valid for spin frequencies less than about 400 Hz (Miller, Lamb & Cook 1998). For  $I = 3 \times 10^{45} \text{ g cm}^2$  (Cook, Shapiro & Teukolsky 1994; Miller, Lamb & Psaltis 1998) and  $\nu_{spin} = 311.8 \text{ Hz}$ , the inferred spin frequency of the star, the kilohertz QPO at  $1329 \pm 4 \text{ Hz}$  constrains  $M$  and  $R$  to  $M \leq 1.9 M_\odot$

and  $R \leq 15.2$  km. These constraints rule out the extremely stiff EOS. A mean-field theory ('L' in Cook, Shapiro & Teukolsky 1994) is ruled out and the tensor interaction EOS ('M' in Cook, Shapiro & Teukolsky 1994) is ruled out except for a very small range of  $R$  and  $M$ . However we note, that this QPO has a single-trial significance of only  $3.5 \sigma$ . To put constraints on the softer EOS the kilohertz QPO must be observed at higher frequencies. For a slow rotating star, 2010 Hz would rule out the 'U'-type EOS (Wiringa, Fiks & Fabrocini 1988) and 1920 Hz would rule out the commonly used 'FPS' EOS (Cook, Shapiro & Teukolsky 1994).

We note that there is no obvious saturation of the kilohertz QPO frequency with respect to  $S_a$ , our chosen indicator of mass accretion rate (see Fig. 4). However the kilohertz QPO at 1329 Hz does deviate from the linear trend seen for the other kilohertz QPOs. Such a saturation where the frequency becomes independent of the chosen mass accretion rate indicator would be an indication for the marginally stable orbit predicted by general relativity (Kluźniak, Michelson & Wagoner 1990; Kaaret, Ford & Chen 1997; Miller, Lamb & Psaltis 1998). Such a saturation has been reported in 4U 1820–30 (Zhang et al. 1998a; Kaaret et al. 1999).

#### 4.5. QPO Frequency Difference

We found that,  $\Delta\nu$ , the frequency difference between the upper and the lower kilohertz QPO peak is constant in 4U 0614+09, confirming the results of Ford et al. (1997a). This matches the prediction of the beat frequency mechanism (e.g. Miller, Lamb & Psaltis 1998) in which  $\Delta\nu$  is equal to the spin frequency and therefore constant. However observations of five sources have shown a sig-

nificant decrease in  $\Delta\nu$  as the frequency of the kilohertz QPOs increases (Sco X–1, van der Klis 1997; 4U 1608–52, Méndez et al. 1998a,b; 4U 1735–44, Ford et al. 1998; 4U 1728–34, Méndez & van der Klis 1999; 4U 1702–42, Markwardt et al. 1999a,b). To examine the trend of  $\Delta\nu$  with increasing QPO frequency in 4U 0614+09 we plot  $\Delta\nu$  vs. the frequency of the lower frequency kilohertz QPO for all these sources in Figure 8. We find that at low QPO frequency ( $< 750$  Hz)  $\Delta\nu$  in 4U 0614+09 is consistent with Sco X–1 and 4U 1608–52 and at high QPO frequency (750–820 Hz) inconsistent ( $2.8$ – $8.0 \sigma$  different). However, we note that one of the points from 4U 0614+09 itself deviates  $11.0 \sigma$  from the trend seen in 4U 0614+09.

#### 5. Acknowledgements

This work was supported by NWO SPINOZA grant 08–0 to E.P.J. van den Heuvel, by the Netherlands Organization for Scientific Research (NWO) under contract number 614–51–002, and by the Netherlands Research School for Astronomy (NOVA). MM is a fellow of the Consejo Nacional de Investigaciones Científicas y Técnicas de la República Argentina. PK acknowledges support from NASA grants NAG5–7405, NAG5–7334, and NAG5–7477. This research has made use of data obtained through the High Energy Astrophysics Science Archive Research Center Online Service, provided by the NASA/Goddard Space Flight Center.

#### REFERENCES

- Barret, D., & Grindlay, J.E., *ApJ*, 440, 841 (1995)  
 Belloni, T., & Hasinger, G., *A&A*, 227, L33 (1990)

- Bildsten, L., ApJ, 438, 852 (1995)
- Brandt, S., Castro-Tirado, A. J., Lund, N., Dremmin, V., Lapshov, I., & Sunyaev, R., A&A, 262, L15 (1992)
- Brandt, S., Ph.D thesis, Danish Space Res. Inst. (1994)
- Breedon, L.M., Turner, M.J.L., King, A.R., Courvoisier, T.J.L., MNRAS, 218, 487 (1986)
- Cook, G.B, Shapiro, S.L., & Teukolsky, S.A., ApJ, 424, 823 (1994)
- Ford, E.C., et al., ApJ, 469, L37 (1996)
- Ford, E.C., et al., ApJ, 475, 123 (1997a)
- Ford, E.C., et al., ApJ, 486, 47 (1997b)
- Ford, E.C., van der Klis, M., & Kaaret, P., ApJL, 498, L41 (1998)
- Ford, E.C., & van der Klis, M., ApJ, 506, 39 (1998)
- Ford, E.C., van der Klis, M., van Paradijs, J., Méndez, M., Wijnands, R., Kaaret, P., ApJ, 508, L155 (1998)
- Grove, J., et al., AIP Conference Proc. 304, p192 (1994)
- Hasinger, G., & van der Klis, M., A&A, 225, 79 (1989)
- Hasinger, G., van der Klis, M., Ebisawa, K., Dotani, T., Mitsuda, K., A&A, 235, 131 (1990)
- Hertz, P., Vaughan, B., Wood, K.S., Norris, J.P., Mitsuda, K., Michelson, P.F., Dotani, T., ApJ, 396, 201 (1992)
- Homan, J., Wijnands, R., van der Klis, M., IAU Circ. No. 7121 (1999)
- Jonker, P.G., Wijnands, R., van der Klis, M., Psaltis, D., Kuulkers, E., Lamb, F.K., ApJ, 499, 191 (1998)
- Kaaret, P., Ford, E., & Chen, K., ApJL, 480, L27 (1997)
- Kaaret, P., Yu, W., Ford, E.C., Zhang, S.N., ApJL, 497, L93 (1998)
- Kaaret, P., Piraino, S., Bloser, P.F., Ford, E.C., Grindlay, J.E., Santangelo, A., Smale, A.P., Zhang, W., ApJL, 520, 37 (1999)
- Kluźniak, W., Michelson, P., & Wagoner, R.V., ApJ, 358, 538 (1990)
- Kuulkers, E., van der Klis, M., Oosterbroek, T., Asai, K., Dotani, T., van Paradijs, J., Lewin, W.H.G., A&A, 289, 795 (1994)
- Kuulkers, E., & van der Klis, M., A&A, 314, 567 (1996)
- Kuulkers, E., van der Klis, M., Oosterbroek, T., van Paradijs, J., Lewin, W.H.G., MNRAS, 287, 495 (1997)
- Langmeier, A., Sztajano, M., Hasinger, G., Truemper, J., Gottwald, M., ApJ, 323, 288 (1987)
- Leahy, D., Darbro, W., Elsner, R.F., Weiskopf, M.C., Kahn, S., Sutherland, P.G., Grindlay, J.E., ApJ, 266, 160 (1983)
- Markwardt, C.B., Strohmayer, T.E., Swank J.H., ApJ, 512, 125 (1999a)
- Markwardt, C.B., Lee, H.C., wank J.H., AAS HEAD, 31:15.01 (Abstr.) (1999b)
- Méndez, M., & van der Klis, M., ApJ, 479, 926 (1997)
- Méndez, M., van der Klis, M., van Paradijs, J., Lewin, W.H.G., Lamb, F.K., Vaughan, B.A., Kuulkers, E., Psaltis, D., ApJ, 485, L37 (1997)
- Méndez, M., et al. ApJ, 494, 65 (1998a)
- Méndez, M., van der Klis, M., Wijnands, R.A.D., Ford, E.C., van Paradijs, J., Vaughan, B.A., ApJ, 505, 23 (1998b)

- Méndez , M., van der Klis, M., Ford, E.C., Wijnands, R., van Paradijs, J., ApJ, 511, 49 (1999)
- Méndez , M., & van der Klis, M., ApJ, 517 , 51 (1999)
- Méndez , M., astro-ph/9903469, to appear in Proceedings of the 19th Texas Symposium in Paris (1999)
- Miller, M.C., Lamb, F., and Psaltis, D., ApJ, 508, 791 (1998)
- Miller, M.C., Lamb, F., and Cook, G., ApJ, 509, 793 (1998)
- Mitsuda, K., Inoue, H., Nakamura, N., Tanaka, Y., PASJ, 41, 97 (1989)
- Morgan, E.H.; Remillard, R.A.; Greiner, J., ApJ, 482, 993 (1997)
- Olive, J.F., Barret, D., Boirin, L., Grindlay, J.E., Swank, J.H., Smale, A.P., A&A, 333, 942 (1998)
- Prins, S., & van der Klis, M., A&A, 319, 498 (1997)
- Psaltis, D., Belloni, T., & van der Klis, M., ApJ, 520, 262 (1999)
- Reig, P., et al., in preparation (1999)
- Remillard, R.A., Morgan, E.H., McClintock, J.E., Bailyn, C.D., Orosz, J.A., ApJ, 522, 397 (1999a)
- Remillard, R.A., McClintock, J.E., Sobczak, G.J., Bailyn, C.D., Orosz, J.A., Morgan, E.H., Levine, A.M., ApJ, 517, 127 (1999b)
- Singh, K.P., & Apparao, K.M.V., ApJ, 431, 826 (1994)
- Smale, A.P., Corbet, R.H.D., Charles, P.A., Menzies, J.W., Mack, P, MNRAS, 223, 207 (1986)
- Smale, A.P., Zhang, W. and White, N.E., ApJL, 483, L119 (1997)
- Swank, J. H., Becker, R. H., Boldt, E. A., Holt, S. S., & Serlemitsos, P. J., MNRAS, 182, 349 (1978)
- Swank, J., astro-ph/9802188, to appear in "The Active X-Ray Sky", eds. L. Scarsi, H. Bradt, P. Giommi, and F. Fiore (1998)
- Stella, L., & Vietri, M., ApJL, 492, L59 (1998)
- Sunyaev, R. and Titarchuk, L., A&A, 86, 121 (1980)
- Titarchuk, L., Lapidus, I., & Muslimov, A., ApJ, 499, 315 (1998)
- Titarchuk, L., & Osherovich, V., ApJL, 518, 95 (1999)
- van der Klis, M., Nature, 316, 225 (1985)
- van der Klis, M., in Timing Neutron Stars, Kluwer Academic Publishers: Boston (1989)
- van der Klis, M., In: "Neutron Stars: Theory and Observations", eds. J. Ventura & D. Pines, NATO ASI Series C, 344, p. 319 (1991)
- van der Klis, M., A&A, 283, 469 (1994a)
- van der Klis, M., ApJS, 92, 511 (1994b)
- van der Klis, M., & van Paradijs, J., A&A, 281, L17 (1994)
- van der Klis, M., Swank, J.H., Zhang, W., Jahoda, K., Morgan, E.H., Lewin, W.H.G., Vaughan, B., van Paradijs, J., ApJL, 469, 1 (1996)
- van der Klis, M., Wijnands, R.A.D., Horne K., Chen W., ApJ, 481, 97, (1997)
- van der Klis, M., in The Many Faces of Neutron Stars, ed. R. Buccheri, J. van Paradijs, & M. A. Alpar (NATO ASI Series C, Vol. 515, Dordrecht: Kluwer), 337 (1998)

- van der Klis, M., in Proc. of the Third William Fairbank Meeting, Rome June 29 - July 4 1998 (1999)
- Wijnands, R.A.D., van der Klis, M., Kuulkers, E., Asai, K., Hasinger, G., *A&A*, 323, 399 (1997a)
- Wijnands, R.A.D., et al., *ApJ*, 490, L157 (1997b)
- Wijnands, R.A.D., van der Klis, M., van Paradijs, J., Lewin, W.H.G., Lamb, F.K., Vaughan, B., Kuulkers, E., *ApJL*, 479, L141 (1997c)
- Wijnands, R.A.D., & van der Klis, M., *ApJL*, 482, L65 (1997)
- Wijnands, R.A.D., & van der Klis, M., *ApJ*, 507, L63 (1998)
- Wijnands, R.A.D., et al., *ApJL*, 493, L87 (1998a)
- Wijnands, R.A.D., van der Klis, M., Méndez, M., van Paradijs, J., Lewin, W.H.G., Lamb, F.K., Vaughan, B., Kuulkers, E., *ApJL*, 495, L39 (1998b)
- Wijnands, R.A.D., & van der Klis, M., *ApJ*, 514, 939 (1999a)
- Wijnands, R.A.D., & van der Klis, M., *astro-ph/9903450* (1999b)
- Wiringa, R.B., Fiks, V., & Fabrocini, A., *Phys. Rev. C*, 38, 1010 (1988)
- Yoshida, K., Mitsuda, K., Ebisawa, K., Ueda, Y., Fujimodo, R., Yaqoob, T., Done, C., *PASJ*, 45, 605 (1993)
- Zhang, W., Giles, A.B., Jahoda, K., Soong, Y., Swank, J.H., Morgan, E.H., *SPIE*, 2006, 324 (1993)
- Zhang, W., Lapidus, I., White, N.E., & Titarchuk, L., *ApJL*, 469, L17 (1996)
- Zhang, W., Smale, A.P., Strohmayer, T.E., Swank, J.H., *ApJ*, 500, L171 (1998a)
- Zhang, W., Jahoda, K., Kelley, R.L., Strohmayer, T.E., Swank, J.H. and Zhang, S.N., *ApJ*, 495, L9 (1998b)

---

This 2-column preprint was prepared with the AAS L<sup>A</sup>T<sub>E</sub>X macros v4.0.

Table 1: 4U 0614+09 RXTE Observations &amp; kilohertz QPO fits

$S_A$	Start Time UTC	$T_{obs}$ (ks)	$T_{res}$ ( $\mu$ s)	Rate (cts/s)	Higher kHz QPO			Lower kHz QPO		
					frequency (Hz)	FWHM (Hz)	rms (%)	frequency (Hz)	FWHM (Hz)	rms (%)
1.14±0.10	26 Feb 1996 08:54	3.5	8	210	-	-	-	-	-	-
1.16±0.09	26 Feb 1996 10:34	1.4	8	210	-	-	-	-	-	-
1.23±0.08	16 Mar 1998 11:45	2.9	122	247	-	-	-	-	-	-
1.24±0.08	8 Aug 1996 03:32	2.6	122	264	-	-	-	-	-	-
1.24±0.09	16 Mar 1998 10:02	3.3	122	246	-	-	-	-	-	-
1.25±0.08	8 Aug 1996 01:50	2.9	122	269	449.4±19.5	120.5±54.5	18.9±3.4	153.4±5.6	16.7±11.4	10.9±2.1
1.26±0.09	17 Mar 1998 11:43	3.0	122	259	499.8±32.9	225.8±98.0	23.9±5.9	-	-	-
1.28±0.08	8 Aug 1996 00:11	2.5	122	273	-	-	-	-	-	-
1.30±0.09	20 Mar 1998 10:23	2.2	122	288	-	-	-	-	-	-
1.32±0.07	10 Oct 1997 13:28	3.0	122	332	-	-	-	-	-	-
1.32±0.07	7 Aug 1996 22:31	3.4	122	286	522.4±9.4	32.6±16.2	10.6±2.7	-	-	-
1.36±0.07	4 Jan 1999 01:26	1.8	122	322	-	-	-	-	-	-
1.38±0.07	7 Aug 1996 20:55	3.4	122	296	555.6±14.9	103.6±50.6	16.7±3.1	-	-	-
1.39±0.07	7 Aug 1996 19:19	3.4	122	296	585.5±32.1	239±139	24.9±5.4	-	-	-
1.40±0.07	23 Dec 1998 21:33	3.1	122	342	547.3±11.9	72.0±37.8	13.1±2.6	-	-	-
1.44±0.07	22 Apr 1996 19:21 <sup>2</sup>	2.6	122	345	-	-	-	-	-	-
1.44±0.07	22 Apr 1996 22:41	3.4	122	343	569.2±25.8	196.6±75.9	19.3±3.8	-	-	-
1.44±0.06	18 Oct 1997 18:21	3.4	122	418	532.±14.0	126.2±77.9	15.4±3.5	-	-	-
1.44±0.07	2 Jan 1999 23:47	1.5	122	345	626.±12.2	84.6±31.2	18.0±2.9	-	-	-
1.44±0.08	22 Apr 1996 20:58 <sup>2</sup>	3.4	122	346	575.9±20.5	131.2±44.0	18.5±2.8	-	-	-
1.49±0.08	13 Mar 1998 11:43	2.9	122	309	695.1±10.1	84.8±26.6	19.0±3.0	-	-	-
1.50±0.06	2 Jan 1999 22:06	1.3	122	368	-	-	-	-	-	-
1.51±0.06	10 Jan 1997 10:49 <sup>2</sup>	1.3	122	430	-	-	-	-	-	-
1.51±0.06	10 Jan 1997 10:16	2.0	122	436	600.3±19.9	211.0±93.4	21.4±4.2	-	-	-
1.51±0.07	13 Mar 1998 10:25	1.9	122	307	657.6±3.5	19.9±8.1	12.7±1.8	-	-	-
1.53±0.05	6 Sep 1997 22:55	2.0	0.95	491	591.4±16.3	133.1±57.9	16.5±2.8	-	-	-
1.55±0.08	13 Apr 1996 09:51 <sup>1</sup>	2.7	8	413	654.6±7.6	37.7±28.5	12.0±2.5	-	-	-
1.56±0.05	18 Mar 1996 09:11	3.4	122	537	568.8±29.3	252±125	15.6±3.6	-	-	-
1.56±0.05	6 Sep 1997 21:20	3.5	0.95	502	639.3±17.4	145.7±70.0	18.1±3.3	-	-	-
1.57±0.07	30 Dec 1998 22:07 <sup>2</sup>	2.6	122	402	644.8±33.7	235±107	22.5±4.9	-	-	-
1.58±0.08	13 Apr 1996 11:32 <sup>1</sup>	2.3	8	422	-	-	-	-	-	-
1.58±0.07	15 Mar 1998 11:44	2.9	122	333	-	-	-	-	-	-
1.58±0.07	18 Mar 1998 13:25	2.6	122	339	706.9±19.0	135.5±60.9	19.1±3.8	-	-	-
1.58±0.06	25 May 1999 05:08 <sup>2</sup>	3.3	122	481	605.9±17.7	136.2±54.5	17.5±3.8	-	-	-
1.60±0.05	6 Sep 1997 17:54	2.8	122	512	623.3±14.2	167.3±55.8	17.8±2.5	-	-	-
1.61±0.05	3 Sep 1997 21:12	2.9	122	517	626.8±13.3	178.6±46.3	19.3±2.3	-	-	-
1.61±0.07	6 Sep 1997 19:28 <sup>1,3</sup>	0.2	0.95	521	581.5±16.2	115.1±45.2	18.1±3.1	-	-	-
1.61±0.07	6 Sep 1997 19:58 <sup>1,3</sup>	1.6	0.95	-	-	-	-	-	-	-
1.61±0.07	6 Sep 1997 23:34 <sup>1,3</sup>	0.3	0.95	-	-	-	-	-	-	-
1.61±0.06	12 Nov 1998 13:46	2.7	122	400	702.7±11.9	72.5±46.7	12.7±2.7	-	-	-
1.63±0.07	23 May 1999 00:23 <sup>1</sup>	3.6	122	481	668.4±15.7	130.2±73.8	18.3±4.1	-	-	-
1.65±0.05	16 Mar 1996 22:25	2.9	122	514	673.7±21.1	224.9±103	18.3±2.9	-	-	-
1.67±0.04	25 Jan 1997 13:39	3.4	122	565	629.2±13.7	156.0±73.1	16.3±2.9	-	-	-
1.67±0.04	15 Aug 1997 00:06	3.2	0.95	583	644.4±8.6	94.6±27.0	13.6±1.6	-	-	-
1.68±0.05	16 May 1997 05:23	3.4	122	570	652.5±8.3	123.5±37.0	16.3±2.0	-	-	-
1.7±0.05	14 Aug 1997 20:51	3.3	0.95	589	663.5±8.5	133.5±28.9	17.2±1.6	-	-	-
1.71±0.04	14 Aug 1997 22:32	3.1	0.95	594	675.0±6.8	92.0±29.4	14.4±1.7	-	-	-
1.72±0.06	19 Mar 1998 10:04	3.3	122	391	799.1±15.1	102.1±36.1	16.2±2.8	-	-	-
1.77±0.04	26 Apr 1996 00:11	3.4	122	453	767.2±9.6	134.7±33.4	20.1±2.4	418.3±1.8	9.7±3.7	6.8±0.9
1.79±0.04	16 Mar 1996 09:11	3.5	8	539	720.0±10.7	168.8±38.8	18.9±2.1	-	-	-
1.79±0.05	24 Dec 1998 21:33	3.3	122	493	754.0±11.9	192.3±73.0	18.1±3.3	-	-	-
1.81±0.05	24 Apr 1996 22:36	3.4	122	474	809.4±4.2	39.3±14.5	12.1±1.7	-	-	-
1.83±0.04	6 Sep 1997 00:16	2.5	0.95	613	751.8±7.7	106.1±22.9	16.5±1.5	-	-	-
1.83±0.04	8 Sep 1997 21:05	3.4	0.95	613	750.4±10.6	153.6±35.0	17.5±1.7	-	-	-
1.83±0.05	31 Dec 1998 22:07	2.4	122	476	831.0±12.3	167.2±61.4	20.5±3.2	533.4±5.9	27.3±22.6	8.1±1.9
1.84±0.06	7 Aug 1996 03:31	2.6	122	436	851.3±23.4	185.7±77.5	18.5±3.9	473.1±10.9	43.9±34.6	10.0±2.5
1.84±0.05	25 Apr 1996 01:47	3.4	122	480	803.6±5.1	65.0±13.5	15.3±1.4	565.3±4.4	20.4±0.3	7.7±1.4
1.85±0.05	16 Mar 1996 10:47	1.0	8	548	-	-	-	-	-	-
1.85±0.04	31 Oct 1998 03:37	3.1	122	510	845.7±6.4	81.8±22.6	15.2±1.8	502.2±11.8	55.1±24.9	9.4±1.8
1.86±0.04	8 Sep 1997 22:39	3.5	0.95	621	777.3±11.4	129.4±27.3	15.0±1.5	-	-	-
1.87±0.04	25 Apr 1996 03:23	3.4	122	493	818.9±9.3	145.2±32.7	20.5±2.2	-	-	-
1.88±0.04	7 May 1997 10:14	2.2	122	671	736.3±14.1	116.6±49.5	13.9±2.2	-	-	-
1.90±0.05	24 Apr 1996 20:59	3.4	122	510	845.7±10.0	115.4±29.0	17.0±1.8	-	-	-
1.94±0.04	24 Apr 1996 19:48	1.9	122	527	853.±10.7	101.4±37.8	14.8±2.4	551.2±3.8	10.7±14.7	6.2±1.5
1.95±0.04	7 Aug 1996 01:50	2.9	122	481	909.7±13.1	95.1±82.6	14.9±5.2	585.8±3.6	18.7±6.3	7.9±1.1
1.98±0.04	24 Apr 1996 14:58	2.0	122	547	881.8±8.1	66.4±23.7	13.6±1.8	561.3±2.5	13.0±9.0	7.3±1.4
1.99±0.04	24 Apr 1996 18:19	2.4	122	549	894.3±3.6	25.6±12.5	10.5±1.5	570.7±3.2	12.3±6.9	7.1±1.3
2.00±0.04	7 Aug 1996 00:10	3.2	122	510	973.5±13.8	132.4±37.4	16.4±2.3	623.6±4.2	42.4±11.3	12.4±1.3
2.01±0.05	24 Apr 1996 19:23	0.9	122	559	871.3±7.2	39.5±11.0	12.4±1.5	582.5±3.5	18.1±11.6	9.8±1.4
2.01±0.05	24 Apr 1996 13:21 <sup>2</sup>	2.1	122	559	894.7±6.5	45.6±19.9	12.9±1.8	581.7±1.5	9.0±4.2	8.6±1.1
2.01±0.04	25 Apr 1996 04:59	3.4	122	558	911.9±5.2	55.8±17.4	12.4±1.5	580.4±3.6	35.2±12.6	10.4±1.3
2.04±0.05	14 Mar 1998 11:43 <sup>2</sup>	2.9	122	524	1024.7±6.3	41.1±30.8	11.0±2.4	695.8±4.5	44.6±12.3	14.2±1.6
2.04±0.04	24 Apr 1996 16:36	1.9	122	570	934.8±7.4	57.1±18.7	12.6±1.8	609.4±3.1	37.1±8.4	13.9±1.2
2.05±0.04	10 Mar 1998 13:24	1.9	122	591	1024.±16.2	109.9±34.0	13.7±2.8	707.6±3.7	42.6±9.7	14.4±1.5
2.06±0.03	6 Aug 1996 22:30	3.4	122	546	987.0±16.2	81.0±31.6	11.1±1.9	679.6±1.6	26.2±5.7	12.7±1.0
2.09±0.04	29 Dec 1998 22:07	2.6	122	631	973.7±20.6	341±109	21.2±4.2	636.6±2.4	31.4±6.3	11.1±0.9
2.13±0.03	6 Aug 1996 21:23	1.6	122	592	1034.4±6.1	34.1±32.1	9.6±2.2	726.7±2.9	39.5±9.3	14.6±1.4
2.14±0.04	10 Mar 1998 11:46	2.8	122	606	1105.0±22.7	230.6±95.5	17.0±3.4	762.6±7.6	83.5±23.8	14.0±1.6
2.14±0.03	9 Mar 1998 10:02	3.1	122	604	-	-	-	748.0±1.7	28.8±4.9	13.0±1.0
2.16±0.04	7 Mar 1998 10:01	3.2	122	628	1066.5±10.4	71.4±29.1	10.1±1.8	738.8±5.1	64.2±10.5	14.2±1.3
2.18±0.04	1 Nov 1998 15:24	3.3	122	654	985.5±5.8	39.4±21.3	7.9±1.2	693.7±3.2	45.4±4.8	13.4±0.8
2.20±0.03	10 Mar 1998 10:02	3.2	122	651	1161.8±4.6	66.7±11.8	13.9±1.2	823.7±10.0	38.1±37.4	6.3±1.4
2.21±0.02	6 Aug 1996 20:55	1.7	122	656	1136.6±6.2	45.2±15.5	10.2±1.5	821.6±21.9	204.2±66.4	16.2±3.1
2.22±0.02	10 Mar 1998 08:22	3.4	122	663	1175.3±6.5	83.7±27.2	13.1±1.5	-	-	-
2.25±0.02	9 Nov 1998 12:24	1.3	122	692	1038.6±7.1	21.5±8.1	6.7±1.5	734.7±1.3	25.8±3.6	14.6±0.9
2.25±0.02	30 Oct 1998 13:57	1.5	122	693	1015.8±11.1	54.6±39.4	9.0±1.1	727.2±0.9	29.6±3.1	14.0±0.7
2.25±0.02	8 Mar 1998 10:20	1.5	122	692	1146.0±3.4	28.4±15.2	9.1±1.7	-	-	-
2.49±0.02	6 Nov 1998 15:23 <sup>2</sup>	2.0	122	873	1221.4±6.2	62.2±13.3	11.1±1.0	-	-	-
2.58±0.02	25 Dec 1998 21:37	3.1	122	936	1217.2±3.1	34.1±9.5	8.4±0.7	-	-	-
2.59±0.03	2 Nov 1998 17:00 <sup>4</sup>	4.9	122	946	1272.6±14.6	89.6±30.5	6.6±0.9	-	-	-
2.59±0.03	5 Nov 1998 15:23 <sup>4</sup>	2.8	122	-	-	-	-	-	-	-
2.59±0.03	8 Nov 1998 13:55 <sup>4</sup>	2.0	122	-	-	-	-	-	-	-
2.64±0.04	31 Oct 1998 19:03 <sup>5</sup>	2.3	122	982	-	-	-	-	-	-
2.64±0.04	3 Nov 1998 16:51 <sup>5</sup>	3.3	122	-	-	-	-	-	-	-
2.64±0.04	4 Nov 1998 18:43 <sup>5</sup>	2.8	122	-	-	-	-	-	-	-
2.78±0.06	27 Dec 1998 21:35 <sup>2</sup>	2.6	122	1089	-	-	-	-	-	-
2.79±0.06	6 Mar 1998 12:00	1.3	122	1092	-	-	-	-	-	-
2.79±0.04	28 Dec 1998 22:06	1.8	122	1094	-	-	-	-	-	-
2.89±0.06	26 Dec 1998 21:36	3.1	122	1172	1329.4±4.2	26.3±13.9	5.1±0.9	-	-	-
2.91±0.06	7 Nov 1998 15:23	2.8	122	1184	-	-	-	-	-	-

Note. — Listed from top to bottom in order of increasing  $S_A$  (position in the hard color vs. intensity diagram) are, the start time (in Universal Time, Coordinated),  $T_{obs}$  (the total useful observing time),  $T_{res}$  (the raw time resolution of the PCA mode we use for making the Fourier power spectra), the background subtracted count rate over five

Table 2: 4U 0614+09 low frequency power spectra fits

$S_a$	$\nu_{break}$ (Hz)	rms (%)	HPN $\alpha_0$	$\alpha_1$	rms (%)	VLPN $\alpha$	Low Frequency frequency (Hz)	Lorentzian FWHM (Hz)	rms (%)	High Frequency frequency (Hz)	Lorentzian FWHM (Hz)	rms (%)
1.14±0.10	0.7±0.1	29.8±2.3	0.08±0.05	1.00±0.02	-	-	6.3±0.5	5.9±1.2	11.2±1.5	-	-	-
1.16±0.09	0.7±0.1	26.3±2.6	-0.06±0.08	1.02±0.03	-	-	6.7±0.6	7.6±1.6	15.9±2.2	-	-	-
1.23±0.08	2.1±0.3	26.4±2.4	0.02±0.05	0.99±0.04	-	-	11.5±1.1	11.6±3.0	12.1±2.0	-	-	-
1.24±0.08	1.8±0.2	29.2±2.0	0.10±0.05	0.97±0.03	-	-	12.2±1.4	9.3±2.9	9.9±1.8	-	-	-
1.24±0.09	2.2±0.2	28.7±2.1	0.01±0.04	0.97±0.03	-	-	12.7±1.4	12.5±3.8	10.9±2.0	-	-	-
1.25±0.08	1.8±0.2	28.3±1.7	-0.03±0.05	0.96±0.03	-	-	11.2±1.1	12.1±2.9	13.2±1.7	-	-	-
1.26±0.09	2.5±0.3	30.2±2.8	-0.01±0.04	0.81±0.02	-	-	13.1±0.8	7.0±4.3	8.9±2.4	-	-	-
1.28±0.08	1.7±0.1	29.2±1.3	-0.08±0.05	0.90±0.03	-	-	13.5±1.3	11.9±2.9	10.9±1.5	-	-	-
1.30±0.09	3.2±0.4	28.9±1.3	0.05±0.04	0.85±0.03	-	-	-	-	-	-	-	-
1.32±0.07	2.0±0.1	28.0±1.2	0.02±0.03	0.88±0.02	-	-	12.4±0.8	11.9±2.4	11.1±1.2	-	-	-
1.32±0.07	3.4±0.5	31.0±0.9	-0.01±0.05	0.89±0.03	-	-	-	-	-	-	-	-
1.36±0.07	3.0±0.3	25.4±2.6	-0.10±0.07	0.93±0.06	-	-	15.3±2.5	17.3±11.4	12.4±6.1	-	-	-
1.38±0.07	5.4±0.4	30.4±1.4	0.04±0.03	0.85±0.03	-	-	-	-	-	-	-	-
1.39±0.07	6.3±1.1	29.4±1.4	0.02±0.04	0.93±0.04	-	-	-	-	-	-	-	-
1.40±0.07	2.1±0.3	26.2±1.1	-0.09±0.05	0.83±0.03	-	-	14.8±1.3	18.9±3.6	13.2±1.4	-	-	-
1.44±0.07	4.7±0.3	30.2±0.7	-0.02±0.04	0.86±0.03	-	-	-	-	-	-	-	-
1.44±0.07	6.1±0.7	27.6±0.9	0.05±0.03	0.89±0.03	-	-	17.1±1.5	10.8±4.8	7.2±2.2	-	-	-
1.44±0.06	4.1±0.2	25.9±1.0	0.07±0.06	0.93±0.06	-	-	16.7±0.6	9.2±3.1	8.5±1.2	-	-	-
1.44±0.07	6.5±0.6	29.2±1.1	-0.03±0.05	0.87±0.03	-	-	-	-	-	-	-	-
1.44±0.08	4.6±0.3	29.1±0.7	0.01±0.04	0.88±0.02	-	-	18.8±0.4	1.6±1.1	4.0±0.8	-	-	-
1.49±0.08	17.2±1.4	27.5±1.6	0.07±0.04	1.00±0.05	-	-	-	-	-	-	-	-
1.50±0.06	10.9±1.7	27.6±1.1	-0.07±0.06	0.97±0.06	-	-	-	-	-	-	-	-
1.51±0.06	7.7±1.3	29.0±1.1	0.04±0.05	0.91±0.05	-	-	-	-	-	-	-	-
1.51±0.06	6.1±0.5	25.6±0.9	0.06±0.03	0.92±0.03	-	-	22.6±1.2	12.4±3.6	8.6±1.2	-	-	-
1.51±0.07	15.5±2.3	27.1±0.8	0.18±0.04	0.99±0.06	-	-	-	-	-	-	-	-
1.53±0.05	4.9±0.4	25.8±0.7	0.04±0.03	0.91±0.03	-	-	18.3±0.9	10.4±4.1	8.0±1.6	-	-	-
1.53±0.08	6.7±1.1	28.8±1.2	-0.06±0.06	0.94±0.05	-	-	21.3±0.3	15.1±1.5	5.1±1.1	-	-	-
1.56±0.05	4.6±0.3	24.2±0.7	0.08±0.02	0.90±0.02	-	-	18.6±0.7	12.8±2.6	9.3±0.8	-	-	-
1.56±0.05	5.7±0.4	25.7±0.5	0.01±0.02	0.89±0.02	-	-	20.7±0.6	7.4±1.7	6.7±0.6	-	-	-
1.57±0.07	12.4±1.4	25.3±0.9	0.04±0.04	0.99±0.05	-	-	-	-	-	-	-	-
1.58±0.08	7.8±1.9	28.6±1.3	0.02±0.05	0.95±0.05	-	-	-	-	-	-	-	-
1.58±0.07	16.4±2.0	27.5±1.7	0.05±0.04	0.85±0.05	-	-	-	-	-	-	-	-
1.58±0.07	15.5±1.8	24.9±1.3	0.06±0.04	1.01±0.06	-	-	-	-	-	-	-	-
1.58±0.06	5.6±0.5	27.1±0.8	0.03±0.04	0.88±0.03	-	-	22.9±1.1	11.9±3.9	7.8±1.2	-	-	-
1.60±0.05	5.8±0.4	24.6±0.6	0.05±0.03	0.85±0.03	-	-	20.5±1.0	15.3±3.4	9.3±1.1	-	-	-
1.61±0.05	6.1±0.3	25.6±0.5	-0.02±0.03	0.88±0.02	-	-	24.2±0.7	8.8±2.0	7.3±0.7	-	-	-
1.61±0.07	8.0±1.1	27.6±0.7	-0.02±0.04	0.90±0.04	-	-	-	-	-	-	-	-
1.61±0.06	12.1±1.0	25.4±0.6	0.05±0.03	0.89±0.04	-	-	-	-	-	-	-	-
1.63±0.07	10.8±1.0	26.3±1.0	0.05±0.04	0.94±0.04	-	-	26.4±0.4	2.6±1.6	4.7±0.9	-	-	-
1.63±0.05	6.8±1.5	24.1±0.9	0.00±0.03	0.87±0.02	-	-	25.5±0.9	12.1±3.4	7.7±0.9	-	-	-
1.67±0.04	7.5±0.6	25.4±0.8	0.05±0.03	0.87±0.02	-	-	25.6±0.7	5.8±3.0	5.1±1.0	-	-	-
1.67±0.04	9.2±0.4	24.6±0.6	0.06±0.02	0.93±0.02	-	-	27.0±0.7	4.3±1.9	4.5±0.7	-	-	-
1.68±0.05	8.4±0.7	24.7±0.5	0.04±0.03	0.88±0.03	-	-	25.3±0.9	8.4±3.3	5.3±1.1	-	-	-
1.71±0.05	10.5±0.6	24.9±0.4	0.03±0.02	0.93±0.02	-	-	27.2±0.5	6.3±1.6	5.6±0.6	-	-	-
1.71±0.04	9.5±0.6	24.0±0.4	0.00±0.03	0.94±0.02	-	-	29.6±0.7	8.4±3.0	5.9±0.8	-	-	-
1.72±0.06	17.8±1.4	23.0±1.4	-0.01±0.04	1.00±0.05	-	-	-	-	-	-	-	-
1.77±0.04	16.4±1.3	22.4±0.8	0.05±0.03	1.03±0.04	-	-	-	-	-	99.2±3.3	27.0±14.3	6.7±1.4
1.79±0.04	12.8±0.8	17.4±0.7	0.01±0.03	0.93±0.03	-	-	31.5±0.7	3.9±1.9	3.7±0.7	-	-	-
1.78±0.05	17.4±1.0	21.0±0.7	0.04±0.03	1.05±0.04	-	-	-	-	-	-	-	-
1.81±0.05	18.6±1.1	22.3±0.8	-0.03±0.03	1.07±0.06	-	-	-	-	-	125.4±4.5	44.0±21.1	8.5±2.1
1.83±0.04	16.6±0.9	22.8±0.4	-0.05±0.04	0.96±0.04	-	-	-	-	-	-	-	-
1.83±0.04	16.4±0.7	21.9±0.4	-0.03±0.03	1.01±0.03	-	-	37.5±0.6	2.0±1.8	2.4±0.6	-	-	-
1.83±0.05	16.2±1.6	21.7±0.7	-0.03±0.05	0.87±0.05	-	-	-	-	-	-	-	-
1.84±0.06	17.4±1.5	21.5±1.1	-0.03±0.05	1.00±0.06	-	-	-	-	-	-	-	-
1.84±0.05	18.6±1.1	22.2±0.8	-0.02±0.03	0.97±0.04	-	-	-	-	-	-	-	-
1.85±0.05	15.0±1.3	21.8±0.8	-0.06±0.06	1.03±0.07	-	-	-	-	-	-	-	-
1.86±0.04	20.5±1.3	20.9±0.7	0.02±0.04	1.05±0.05	-	-	-	-	-	-	-	-
1.86±0.04	16.0±0.7	22.1±0.4	-0.01±0.02	0.98±0.03	-	-	-	-	-	-	-	-
1.87±0.04	18.4±1.2	21.6±0.6	-0.02±0.04	0.97±0.04	-	-	-	-	-	-	-	-
1.88±0.04	14.0±0.8	22.2±0.6	-0.04±0.03	0.98±0.03	-	-	-	-	-	-	-	-
1.90±0.05	20.2±1.1	18.6±1.0	-0.07±0.04	1.25±0.13	-	-	-	-	-	-	-	-
1.94±0.04	19.9±1.7	19.8±0.6	0.04±0.05	1.01±0.07	-	-	-	-	-	-	-	-
1.95±0.04	25.0±1.5	15.1±0.9	-0.06±0.05	1.82±0.35	-	-	-	-	-	115.3±2.7	25.6±12.2	8.0±1.5
1.98±0.04	20.7±1.4	18.4±0.6	-0.10±0.06	1.07±0.08	-	-	-	-	-	-	-	-
1.99±0.04	20.7±1.2	18.2±0.5	-0.09±0.05	1.10±0.07	-	-	-	-	-	-	-	-
2.00±0.04	26.6±1.6	16.1±0.8	-0.04±0.06	1.30±0.16	-	-	-	-	-	158.0±2.7	22.3±11.1	6.7±1.1
2.01±0.05	19.5±7.0	19.0±0.8	0.02±0.08	0.70±0.12	-	-	-	-	-	-	-	-
2.01±0.05	24.6±1.7	18.6±0.8	-0.12±0.08	1.12±0.10	-	-	-	-	-	-	-	-
2.01±0.04	23.0±1.3	18.6±0.5	0.02±0.03	1.06±0.06	-	-	-	-	-	-	-	-
2.04±0.05	23.5±3.5	15.2±0.9	-0.19±0.12	1.15±0.15	-	-	-	-	-	-	-	-
2.04±0.04	23.2±1.1	17.2±0.6	-0.19±0.07	1.24±0.10	-	-	-	-	-	-	-	-
2.05±0.04	26.7±3.8	15.4±0.8	-0.26±0.17	1.02±0.14	-	-	-	-	-	-	-	-
2.06±0.03	30.5±1.2	10.6±0.8	-0.36±0.12	4.24±1.28	-	-	-	-	-	119.2±16.1	143.7±43.7	13.8±1.8
2.09±0.04	27.9±1.0	12.0±0.8	-0.25±0.07	2.85±0.62	-	-	-	-	-	138.0±5.3	97.4±28.9	10.9±1.3
2.13±0.03	30.3±1.3	8.2±0.5	1.64±0.48	5.81±1.57	-	-	-	-	-	143.0±10.6	133.0±41.3	13.8±1.4
2.14±0.04	29.5±3.8	13.6±0.6	-0.25±0.13	1.24±0.19	-	-	-	-	-	-	-	-
2.14±0.03	31.0±2.1	12.6±0.6	-0.43±0.14	1.50±0.20	-	-	-	-	-	-	-	-
2.16±0.04	33.2±1.6	10.1±0.4	-0.33±0.11	3.00 [Fix4]	-	-	-	-	-	143.0±4.0	60.7±14.1	9.4±0.8
2.18±0.04	31.5±1.1	10.6±0.4	-0.43±0.10	3.90±0.73	-	-	-	-	-	135.3±5.2	70.6±23.3	9.8±1.1
2.20±0.03	29.3±0.9	11.6±0.6	-0.90±0.20	1.86±0.22	-	-	-	-	-	-	-	-
2.21±0.02	34.0±2.7	8.8±0.7	-0.79±0.28	4.54±1.43	-	-	-	-	-	115.0±10.5	101.9±49.1	11.1±1.8
2.22±0.02	29.3±1.6	11.8±0.6	-0.62±0.15	1.72±0.23	-	-	-	-	-	-	-	-
2.23±0.02	27.5±2.5	12.8±0.8	-0.40±0.17	1.44±0.24	-	-	-	-	-	-	-	-
2.25±0.02	32.8±1.9	12.9±0.7	-0.56±0.18	1.65±0.26	-	-	-	-	-	-	-	-
2.25±0.02	29.2±4.2	11.8±0.9	-0.33±0.21	1.07±0.24	-	-	-	-	-	-	-	-
2.49±0.02	24.6±10.0	9.8±0.7	-0.28±0.25	0.99±0.19	0.9±0.2	2.07±0.63	-	-	-	-	-	-
2.58±0.02	27.8±4.8	9.6±0.5	-0.35±0.21	1.26±0.25	0.5±0.2	1.93±1.29	-	-	-	-	-	-
2.59±0.03	28.8±1.6	6.0±0.3	-0.29±0.09	3.01±0.76	1.2±0.1	1.70±0.13	-	-	-	118.3±2.4	50.9±8.2	6.7±0.5
2.64±0.04	30.7±1.6	5.5±0.2	-0.16±0.08	5.97±3.06	1.5±0.1	1.52±0.08	-	-	-	113.0±1.6	36.1±4.2	6.9±0.3
2.78±0.06	31.1±3.8	5.2±0.5	-0.09±0.14	5.10±4.00	1.3±0.2	1.62±0.22	-	-	-	108.8±2.6	27.5±8.7	6.6±0.7
2.79±0.06	-	<6.9	-	-	1.4±0.2	2.11±0.27	-	-	-	-	-	-
2.79±0.04	44.9±0.7	13.6±0.3	-0.28±0.03	7.47±1.08	1.0±0.1	1.48±0.23	-	-	-	106.3±4.4	59.4±18.9	7.3±0.7
2.89±0.06	43.1±0.4	13.5±0.2	-0.44±0.02	5.40±0.42	2.1±0.1	1.76±0.07	-	-	-	97.4±3.0	25.1±9.3	3.9±0.5
2.91±0.06	39.6±10.6	3.1±0.8	-0.54±0.94	4.85±3.57	3.2±0.2	1.93±0.10	-	-	-	-	-	-

Note. - Listed from top to bottom in order of increasing  $S_a$  (position in the hard color vs. intensity diagram) are, the fit parameters of the High Frequency Noise (HPN) with  $\alpha_0$  and  $\alpha_1$  the powerlaw indices before and after the break, the Very Low Frequency Noise (VLPN) with  $\alpha$  the powerlaw indices, the 6-38 Hz Lorentzian and the 97-158 Hz Lorentzian. In these fits no channel cuts were applied.

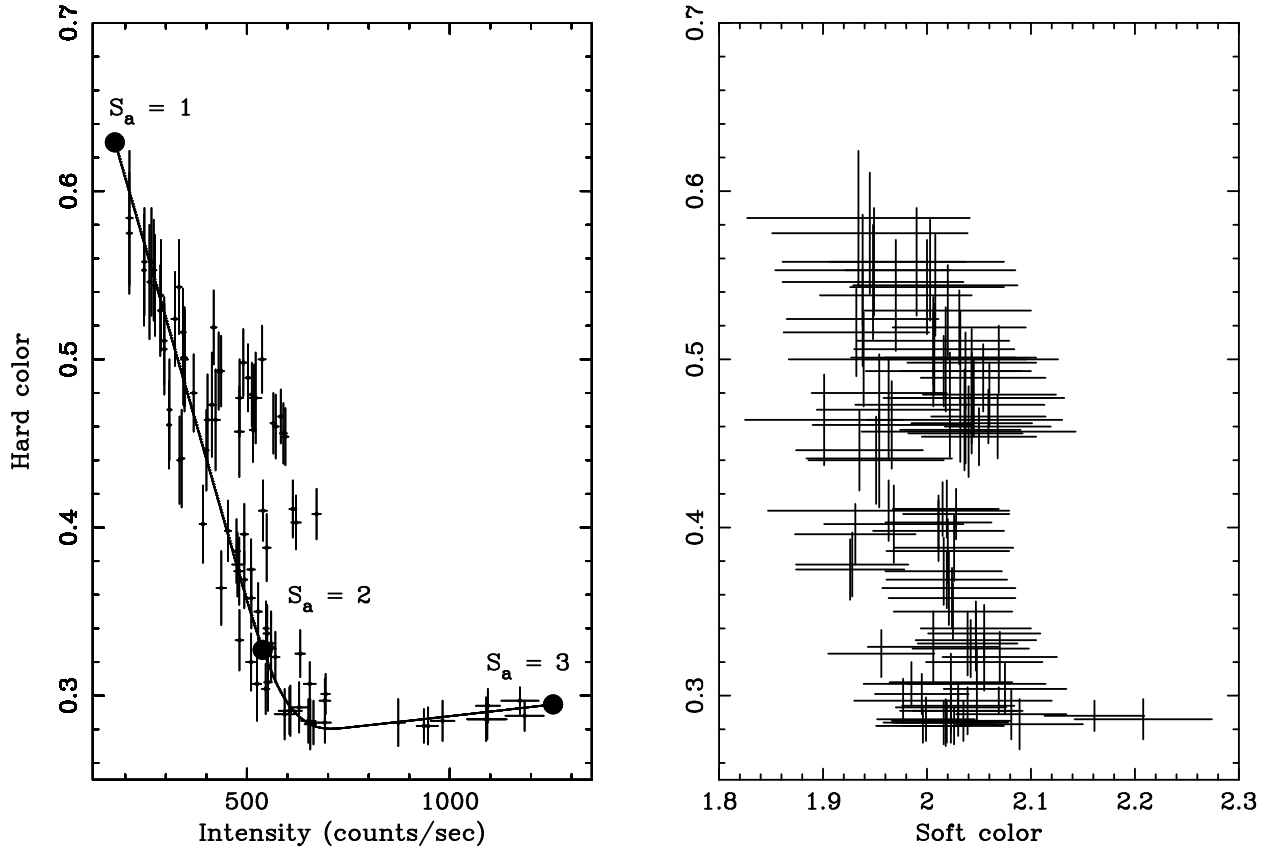


Fig. 1.— Hard color vs. intensity (left panel) and soft color (right panel) for 4U 0614+09. Hard color is defined as the ratio of count rates in the energy bands 9.7–16.0/6.0–9.7 keV. Soft color is defined as the ratio of count rates in the energy bands 3.5–6.0/2.0–3.5 keV. Intensity is defined as the count rate in the energy band 2.0–16.0 keV. Each point is an average over one observation (typically 2500 s). Circles in the left panel indicate values of  $S_a$  along the spline curve (see text).

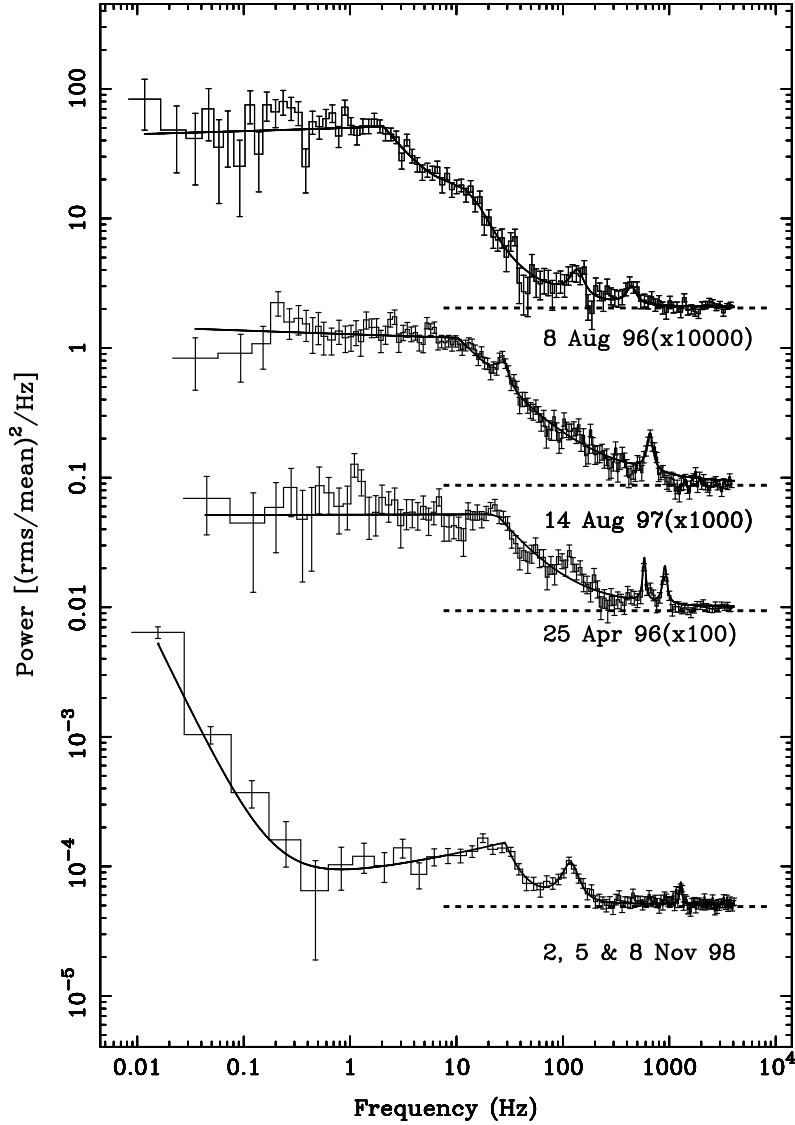


Fig. 2.— Representative power density spectra of 4U 0614+09 for four observations plotted from top to bottom in order of increasing  $S_a$  value,  $S_a$  is respectively 1.25, 1.71, 2.01 and 2.59. The power spectra are for the full energy band of the PCA. We subtract a constant value, somewhat less than the Poisson level and renormalize each spectrum to get fractional squared rms per Hz. The Poisson level is indicated for each spectrum with a dashed line. For clarity each spectrum is multiplied by a constant as indicated. Fit functions are shown which consist of a power-law at low frequency, a broken power-law, a low frequency Lorentzian, a Lorentzian near 100 Hz and kilohertz QPOs. The 25 April 1996 spectral fit does not include a  $\sim 100$  Hz Lorentzian, since it was less than  $3\sigma$  significant.

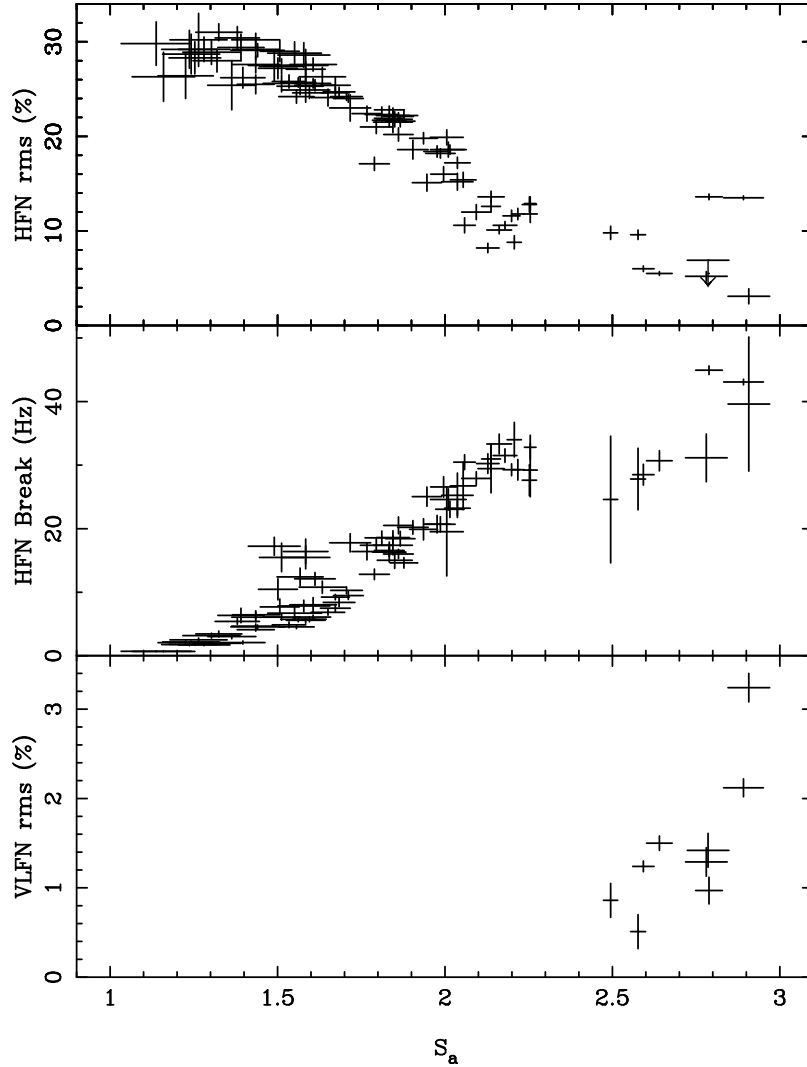


Fig. 3.— Parameters of the fit to the power spectra versus  $S_a$ , the position in the hard color vs. intensity diagram (Fig. 1). The plots are rms fractional amplitude (0.1–400 Hz) of the high frequency noise (broken power-law), the frequency of the break in this component, and the rms fraction (0.01–1 Hz) of the very low frequency noise.

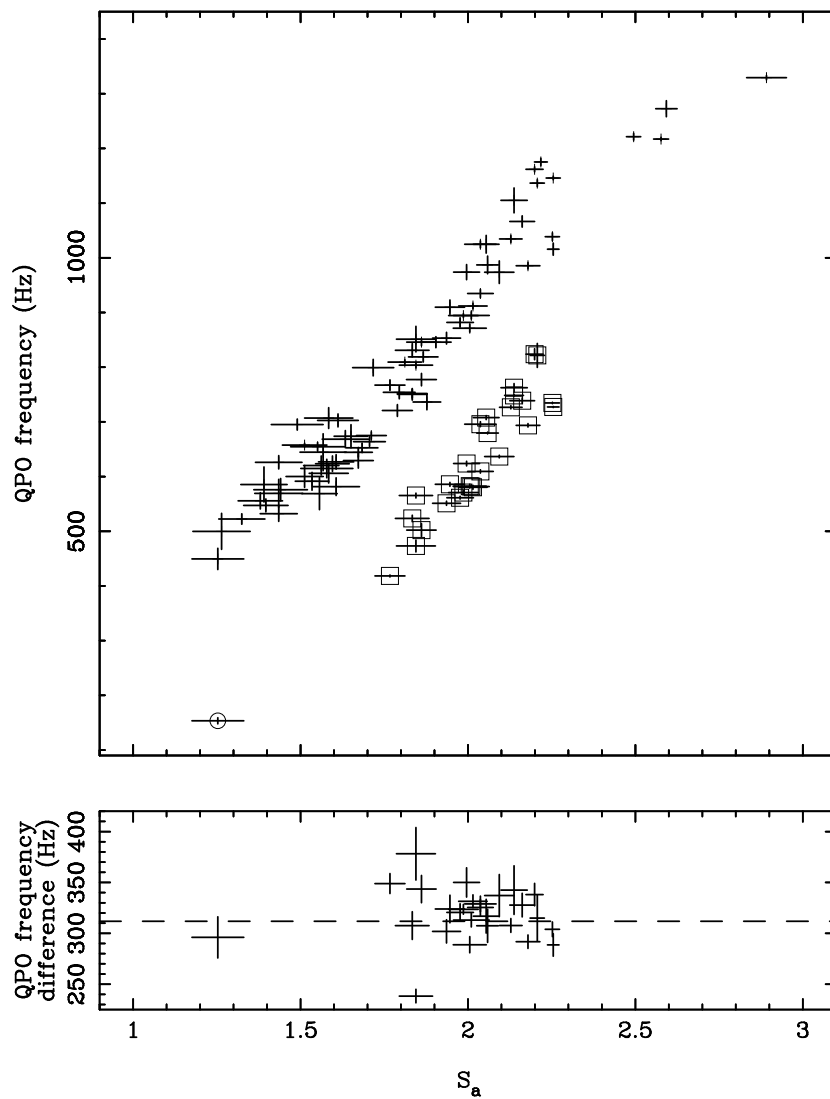


Fig. 4.— Frequency of the kilohertz QPOs vs.  $S_a$  (top) and difference in frequency between double QPOs vs.  $S_a$  (bottom). Plusses represent the higher frequency peak, squares the lower one. The circle marks the case where the QPO can be identified as either the lower kilohertz QPO or the 97–158 Hz Lorentzian (see text and Fig. 5).

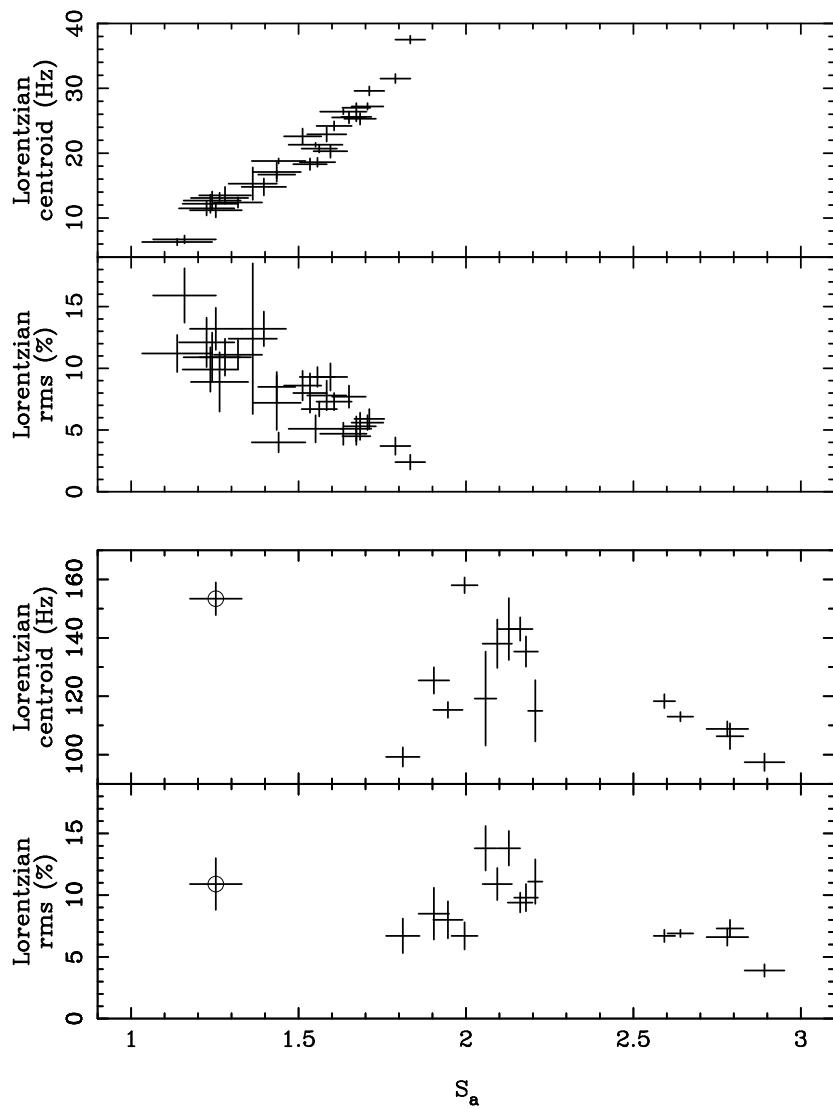


Fig. 5.— Centroid frequency and rms fractional amplitude of the 6–38 Hz (top) and 97–158 Hz (bottom) Lorentzian vs.  $S_a$ . The circle marks the case where the QPO can be identified as either the lower kilohertz QPO or the 97–158 Hz Lorentzian (see text and Fig. 4).

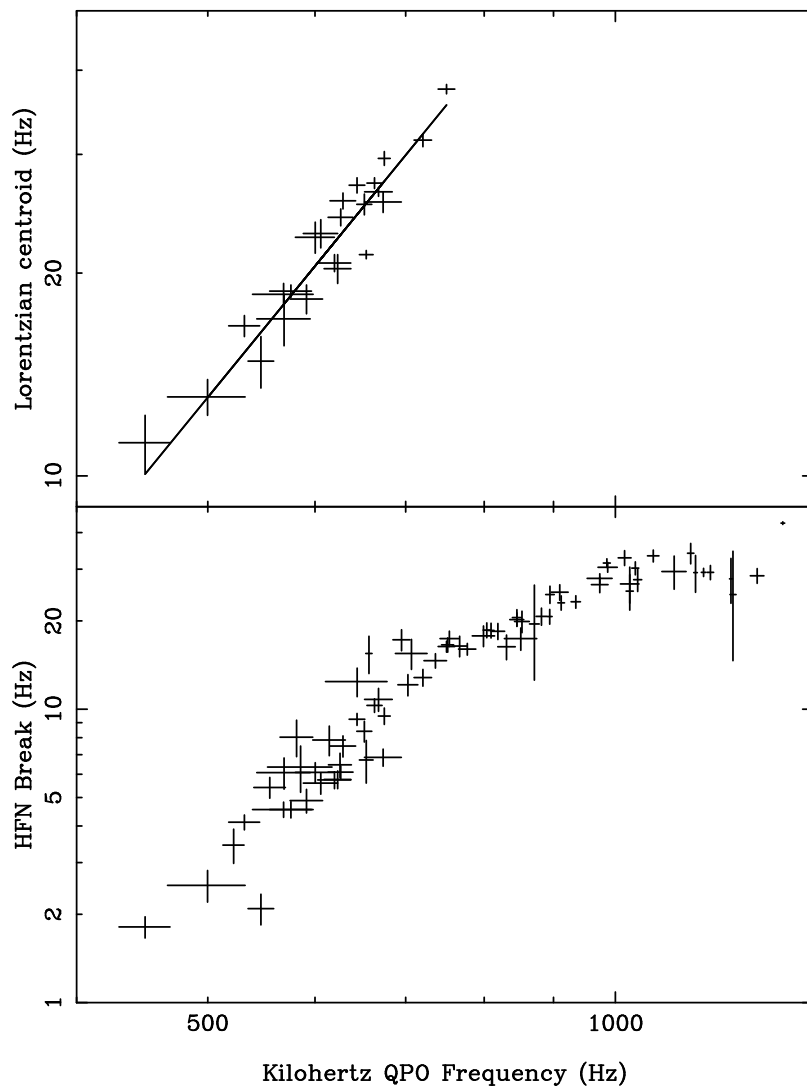


Fig. 6.— Frequency of the Lorentzian at low frequencies (top) and the break frequency of the broken power-law function (bottom) versus the frequency of the upper kilohertz QPO. The function shown is a power-law with index 2.46.

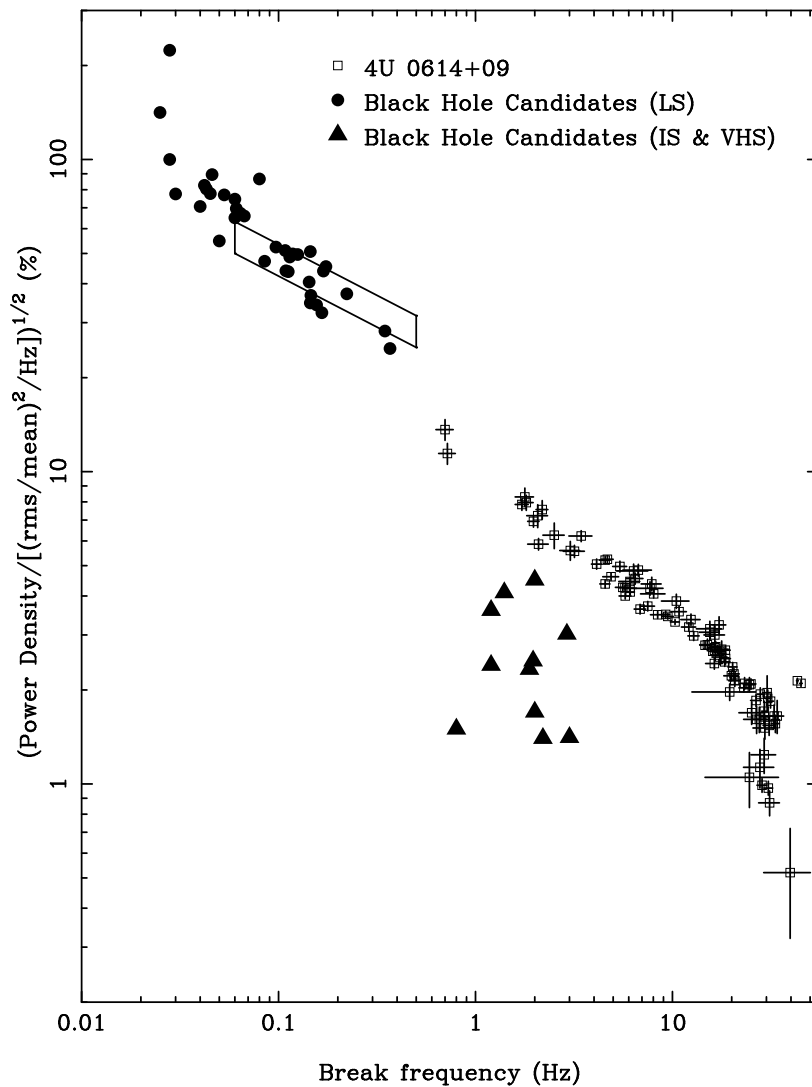


Fig. 7.— Power density of the broken power-law component at the break vs. frequency of the break. The filled points and the marked region are from five different black hole candidates (Méndez & van der Klis 1997 and references therein). The filled circles and the marked region are observations in the low state and the filled triangles are from the intermediate and very high states. The open squares are the points from 4U 0614+09.

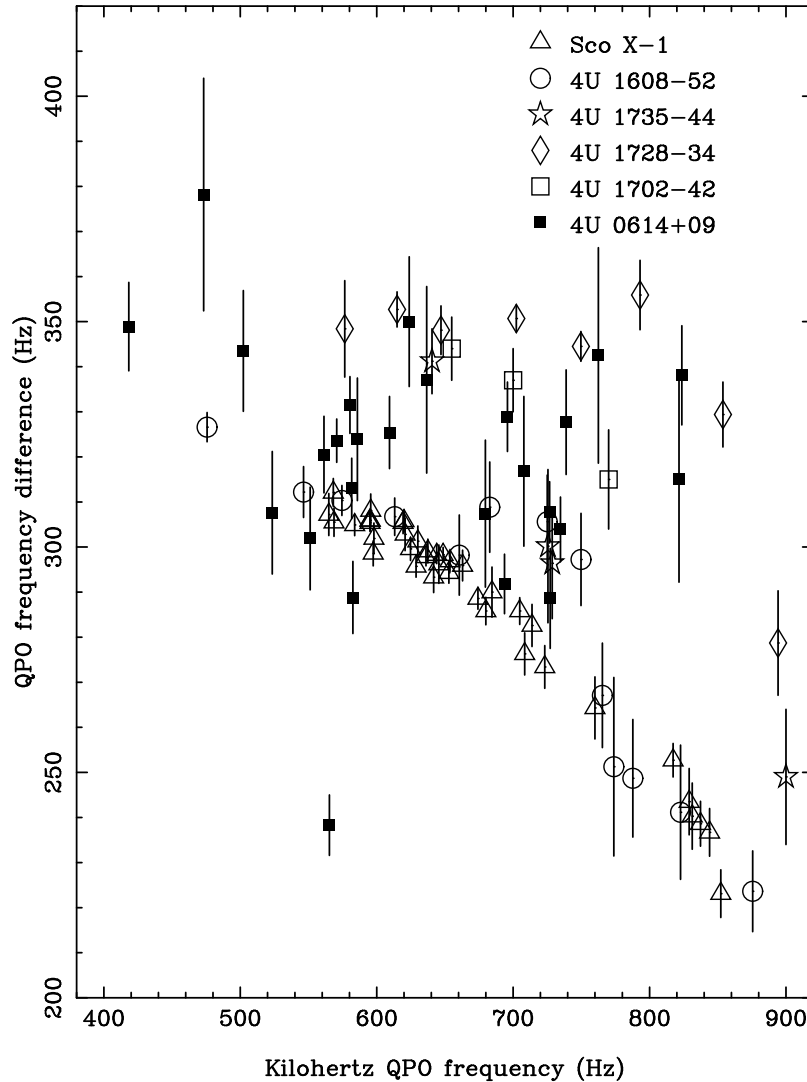


Fig. 8.— The difference in frequency between double kilohertz QPOs vs. the frequency of the lower kilohertz QPOs for four different sources. The open triangles are the points from Sco X-1 (van der Klis et al. 1997), the open circles are the points from 4U 1608-52 (Méndez et al. 1998), the open stars are the points from 4U 1735-44 (Ford et al. 1998; Wijnands et al. 1998b), the open diamonds are the points from 4U 1728-34 (Méndez & van der Klis 1999), the open squares are the points from 4U 1702-42 (Markwardt et al. 1999a,b) and the filled squares are the points from 4U 0614+09 (this paper).